Centimeter-sized single-orientation monolayer hexagonal boron nitride with or without nanovoids

Cun, Huanyao ; Hemmi, Adrian ; Miniussi, Elisa ; Bernard, Carlo ; Probst, Benjamin ; Liu, Ke ; Alexander, Duncan T L ; Kleibert, Armin ; Mette, Gerson ; Weinl, Michael ; Schreck, Matthias ; Osterwalder, Jürg ; Radenovic, Aleksandra ; Greber, Thomas

Abstract: Large-area hexagonal boron nitride (h-BN) promises many new applications of two-dimensional materials, such as the protective packing of reactive surfaces or as membranes in liquids. However, scalable production beyond exfoliation from bulk single crystals remained a major challenge. Single-orientation monolayer h-BN nanomesh is grown on 4 in. wafer single crystalline rhodium films and transferred on arbitrary substrates such as SiO2, germanium, or transmission electron microscopy grids. The transfer process involves application of tetraoctylammonium bromide before electrochemical hydrogen delamination. The material performance is demonstrated with two applications. First, protective sealing of h-BN is shown by preserving germanium from oxidation in air at high temperatures. Second, the membrane functionality of the single h-BN layer is demonstrated in aqueous solutions. Here, we employ a growth substrate intrinsic preparation scheme to create regular 2 nm holes that serve as ion channels in liquids.

DOI: https://doi.org/10.1021/acs.nanolett.7b04752

Originally published at:
Cun, Huanyao; Hemmi, Adrian; Miniussi, Elisa; Bernard, Carlo; Probst, Benjamin; Liu, Ke; Alexander, Duncan T L; Kleibert, Armin; Mette, Gerson; Weinl, Michael; Schreck, Matthias; Osterwalder, Jürg; Radenovic, Aleksandra; Greber, Thomas (2018). Centimeter-sized single-orientation monolayer hexagonal boron nitride with or without nanovoids. Nano letters, 18(2):1205-1212.
DOI: https://doi.org/10.1021/acs.nanolett.7b04752

Centimeter-Sized Single-Orientation Monolayer h-BN with or without Nanovoids

Huanyao Cun,[*,†,‡] Adrian Hemmi,[†] Elisa Miniussi,[†] Carlo Bernard,[†] Benjamin Probst,[¶] Ke Liu,[‡] Duncan Alexander,[§] Armin Kleibert,[‖] Gerson Mette,[†,⊥] Michael Weinl,[#] Matthias Schreck,[#] Jürg Osterwalder,[†] Aleksandra Radenovic,[‡] and Thomas Greber[†]

†*Physik-Institut, Universität Zürich, 8057 Zürich, Switzerland*

‡*Institute of Bioengineering, EPFL, 1015 Lausanne, Switzerland*

¶*Department of Chemistry, Universität Zürich, 8057 Zürich, Switzerland*

§*Centre Interdisciplinaire de Microscopie Électronique, EPFL, 1015 Lausanne, Switzerland*

‖*Swiss Light Source, Paul Scherrer Institut, 5232 Villigen, Switzerland*

⊥*Fachbereich Physik, Philipps-Universität Marburg, 35037 Marburg, Germany*

#*Institut für Physik, Universität Augsburg, 86159 Augsburg, Germany*

E-mail: huanyao.cun@epfl.ch

Abstract

Large-area hexagonal boron nitride (h-BN) promises many new applications of two-dimensional materials, like the protective packing of reactive surfaces or as membranes in liquids. However, scalable production beyond exfoliation from bulk single crystals remained a major challenge. Single orientation monolayer h-BN nanomesh is grown on 4-inch wafer single crystalline rhodium films and transferred on arbitrary substrates like SiO_2, germanium or transmission electron microscopy (TEM) grids. The transfer process involves application of tetraoctylammonium bromide before electrochemical hydrogen delamination. The material performance is demonstrated with two applications. First, protective sealing of h-BN is shown by preserving germanium from oxidation in air at high temperatures. Second, the membrane functionality of the single h-BN layer is demonstrated in aqueous solutions. Here we employ a growth substrate intrinsic preparation scheme to create regular 2 nm holes, which serve as ion channels in liquids.

Keywords: Hexagonal boron nitride, 2D materials, chemical vapor deposition, nanoporous membranes, electrochemical delamination

Introduction

Two-dimensional (2D) materials are expected to significantly widen the prospects for condensed matter systems,[1] to unlock new functionalities in optoelectronics,[2] or ionic transport.[3–5] However, if the materials shall become useful they have to be produced in a scalable way. This means that the exfoliation procedure of 2D flakes from 3D single crystals has to be replaced by processes that yield large-area material. This also applies to hexagonal boron nitride (h-BN) that emerges to be ideal for the encapsulation of graphene-based electronic devices,[6] or that is a promising membrane material in liquids.[3,4] Previous reports on transfer of chemical vapor deposition (CVD) h-BN by H_2 "bubbling" delamination method[7–9] show that the transfer-size was limited to the micrometer flakes.[7] Recent work reports the transfer of large-area multilayer h-BN via the etching of the sapphire substrates.[8] Up to date the transfer of large-area h-BN from metal growth substrates remained an unsolved problem. Here we report on a transfer process of large-area single layer h-BN with single orientation that is grown on 4-inch wafer-scale single crystalline Rh(111) films. The transfer of continuous layers is evidenced for the bare eye with oxidation protection experiments of germanium. The two-step transfer protocol involves electrochemical tetraoctylammonium ion (TOA^+) treatment prior to a hydrogen "bubbling" at the interface of h-BN and metal substrates. It is reliable (high transfer rates above 90%) and gentle since the transferred h-BN layers not only maintain single crystal orientation, but also preserve surface modifications like 2 nm voids that rely on the growth substrates.

As a growth substrate we employ twin-free single-crystalline Rh(111) thin films on 4-inch Si(111) wafers. A corrugated h-BN layer is grown in ultra-high vacuum (UHV) by CVD.[10,11] The corrugation appears as a "mesh"-superstructure with "pores" of about 2 nm diameter, where the BN is closely attached to the substrate, and a surrounding "wire" region with a weaker bonding and a larger layer-substrate distance (Figure 1a).[12–14] This nanomesh surface is stable in air and in liquids,[13,15] and its corrugation can be switched on and off via hydrogen-intercalation either in vacuum[16] or in liquids.[4] With additional preparation steps, single 2 nm voids are fabricated with the "can-opener" effect to form a surface with uniformly distributed voids in the h-BN layer,[17,18]

termed *voidal* boron nitride (v-BN). The functionality of the freestanding v-BN material is demonstrated by immersion of such nanoporous membranes in aqueous solutions and the measurement of ion conductivity.

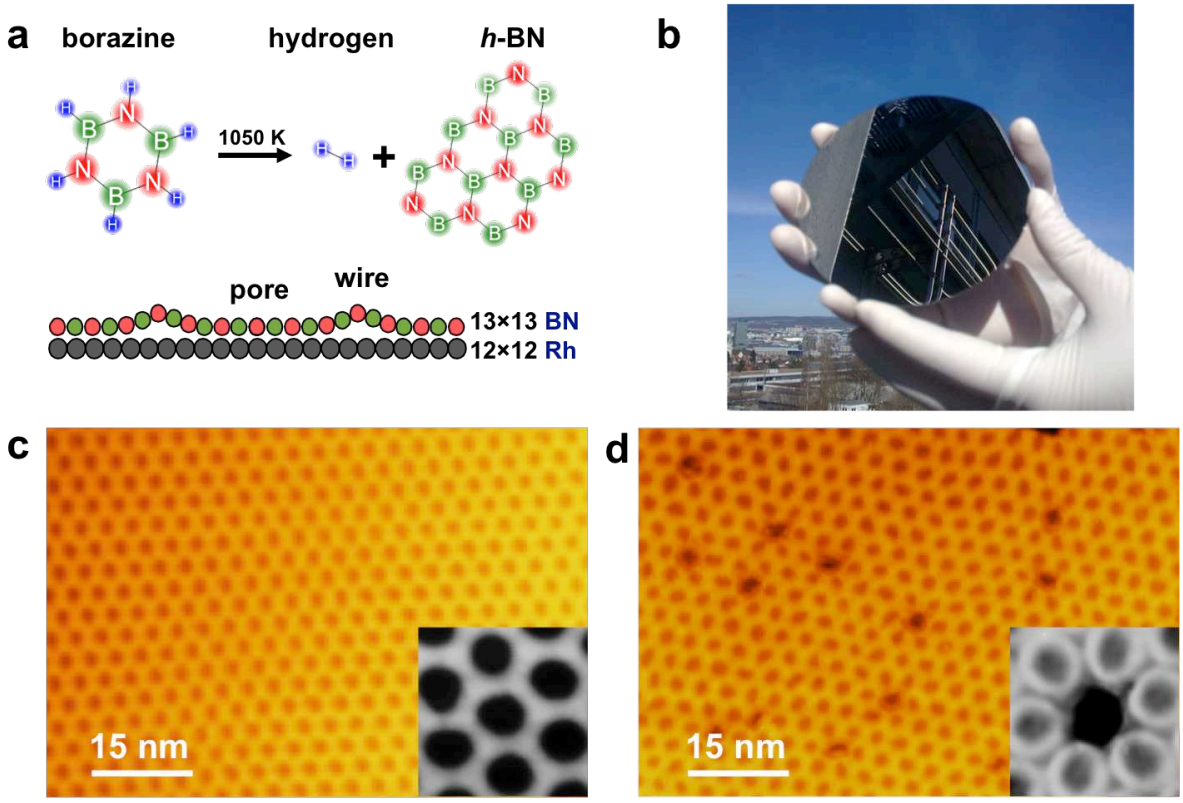

Figure 1: **h-BN nanomesh on Rh(111) with and without 2 nm voids.** (a) Chemical structure of the borazine $(HBNH)_3$ precursor and its decomposition to form a h-BN monolayer and H_2 gas on a hot Rh(111) surface. The h-BN corrugation is caused by the lattice mismatch that accommodates 13×13 BN on 12×12 Rh units. (b) Photograph of a 4-inch wafer single-crystalline Rh(111) thin film substrate in Zürich air, on which the nanomesh is grown. (c) Room temperature STM images of pristine h-BN nanomesh on Rh(111), U_t = -1.20 V, I_t = 0.50 nA. (d) Multiple 2 nm voids at pore sites generated by the "can-opener" effect after annealing of h-BN/Ar/Rh(111) to 900 K, U_t = -1.20 V, I_t = 0.50 nA. The two right-bottom insets show 9 × 9 nm^2 zoom-ins of pristine h-BN nanomesh (c) and voidal v-BN (d).

Results and Discussion

Pristine h-BN monolayers are prepared by the high-temperature CVD method with borazine $(HBNH)_3$ as precursor on single-crystalline Rh(111)/yttria-stabilized zirconia(YSZ)/Si(111) substrates at

1050 K.[11,12] The sample fabrication is scaled up to 4-inch wafers (Figure 1b) and the quality of the h-BN is comparable with the one fabricated on Rh(111) single crystals (Figure 1c).[11] The v-BN is prepared by exposing h-BN/Rh(111) to low energy Ar ions followed by a subsequent annealing procedure.[17,19] The ion bombardment generates vacancy defects in the boron nitride layer, which upon annealing to 900 K leads to the "can-opener" effect, $i.e.$, the formation of 2 nm voids in the h-BN layer,[18] as shown in the scanning tunneling microscopy (STM) image in Figure 1d.

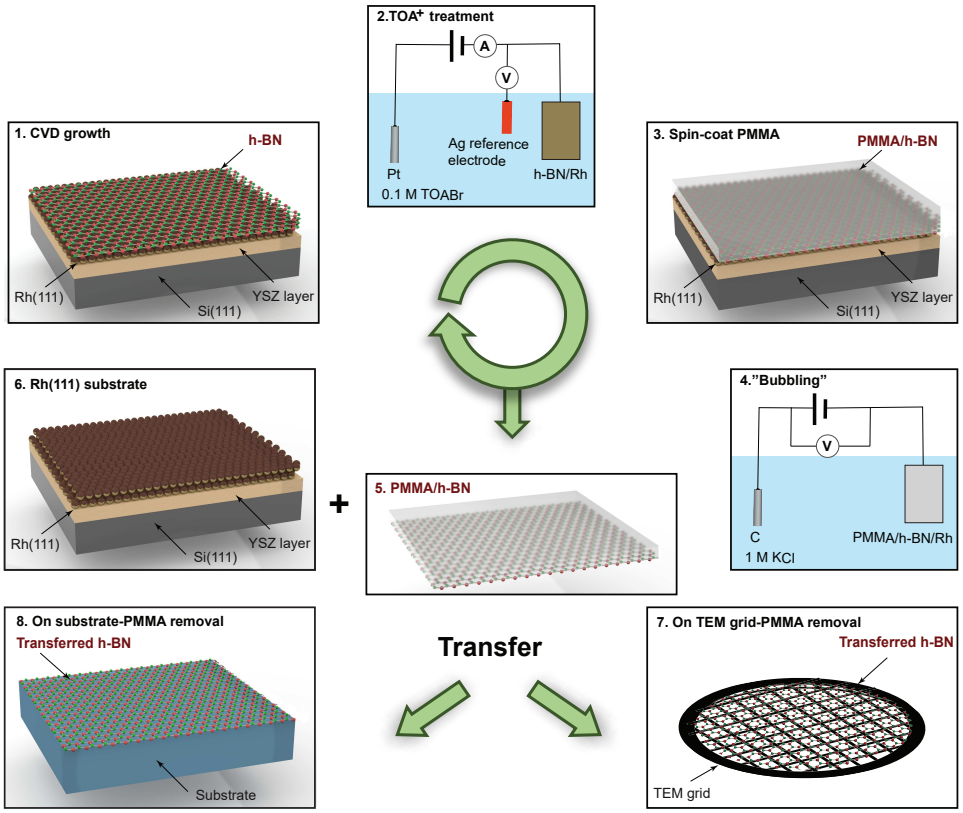

Figure 2: **Two-step TOA$^+$-assisted electrochemical transfer process of h-BN.** (1) Structure of h-BN/Rh(111) film sample. On a Si(111) wafer, an yttria-stabilized zirconia layer (YSZ) (40 nm), Rh(111) (150 nm), and a h-BN monolayer (with or without nanovoids) are grown. (2) First step of the transfer procedure: TOA$^+$-treatment in a three-electrode setup, consisting of a h-BN/Rh sample as working electrode, a Pt wire as counter electrode and an Ag wire as reference electrode in 0.1 M TOABr/acetonitrile solution. (3) TOA/h-BN/Rh sample is spin-coated with PMMA. (4) The second step includes a two-electrode setup with the PMMA/TOA/h-BN/Rh sample as working electrode and a graphite rod as counter electrode in a 1.0 M KCl solution. H_2 bubble evolution between h-BN and Rh substrate lifts the PMMA/TOA/h-BN monolayer (shown in 5). (6) Rh(111) substrate after h-BN transfer can be used for another cycle of h-BN growth (1). The PMMA/h-BN films are transferred on TEM grids (7) and on SiO_2/Si or Ge substrates (8), followed by PMMA removal.

Figure 2 is a schematic illustration of the transfer procedure for single layer h-BN. After UHV-CVD growth (Figure 2-1), the h-BN samples are introduced into a three-electrode setup in a tetraoctylammonium bromide (TOABr)/acetonitrile solution (Figure 2-2).[20] The reference potential is kept at -1.9 V for a thorough diffusion of molecules and ions in the solution and for enabling chemical reactions on the electrodes. This TOA^+-treatment step ensures transfer rates above 90%, while omission of it typically yields transfer rates below 10%, as shown in the Figure S1 in Supporting Information (SI). Subsequently, the TOA-treated sample (TOA/h-BN/Rh) is spin-coated with a polymethylmetacrylate (PMMA) film (Figure 2-3), followed by electrochemical hydrogen intercalation[4] and subsequent "bubbling" delamination[21,22] (Figure 2-4). Finally, the delaminated PMMA/TOA/h-BN film in Figure 2-5 may be transferred to an arbitrary substrate.

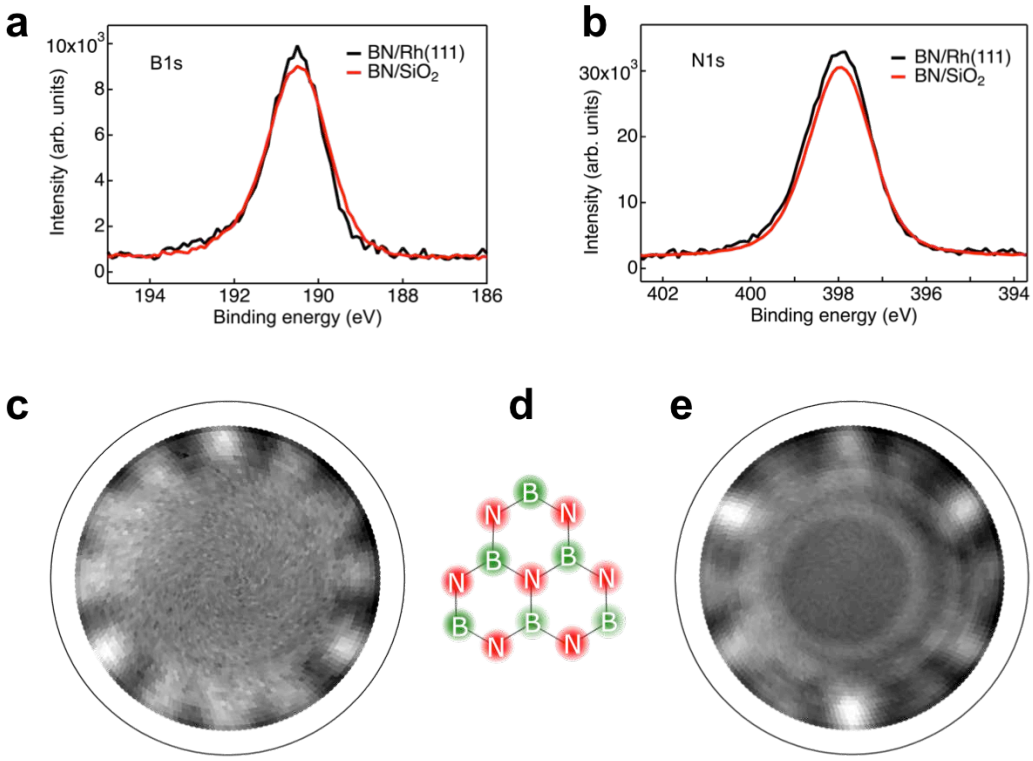

Figure 3: **Mg Kα XPS and XPD ($\hbar\omega = 1253.6$ eV) of h-BN before and after TOA^+-assisted transfer.** (a & b) XPS of B1s and N1s core levels on Rh before (black) and after transfer on 80 nm SiO_2/Si (red). The transfer rate is above 95%. (c & e) X-ray photoelectron diffraction patterns of B1s (c) and N1s (e) of transferred h-BN layer on amorphous SiO_2. The three-fold symmetry indicates a single orientation of the h-BN lattice as depicted in (d).

After transfer, the remaining Rh substrates, as indicated in Figure 2-6, can be recycled in order to regrow h-BN where the quality of the regrown h-BN monolayer stays high (Figure S2 in SI)). In the following, we report transfer results on transmission electron microscopy (TEM) grids (Figure 2-7), on SiO_2 and on Ge(111) wafers (Figure 2-8).

To characterize the transferred PMMA/TOA/h-BN layer, they are placed onto SiO_2/Si substrates and annealed in vacuum to 650 K. The thickness of the 80 nm SiO_2 is chosen to maximize the optical contrast of h-BN[23] and to still allow good electron spectroscopy results by avoiding strong sample charging. Figure 3a and 3b show the x-ray photoelectron spectroscopy (XPS) spectra of B1s and N1s before (black) and after (red) transfer (the survey spectra are shown in Figure S3 in SI). We define the transfer rate as the ratio of the XPS intensities of transferred BN and pristine BN (B1s and N1s) (see section 4 in SI). The XPS results indicate that 95% of the h-BN monolayer is transferred, which fits well with the optical microscopy observation of intact layers (Figure S5 in SI). The angle scanned x-ray photoelectron diffraction (XPD) of B1s and N1s in Figure 3c and 3e indicate a flat single orientation h-BN monolayer transferred onto amorphous SiO_2. The three-fold symmetry with the 3 grazing angle scattering intensity maxima that are rotated by 60 degree between nitrogen and boron are known from h-BN/Ni(111)[24] and h-BN/Rh(111).[25] Comparison of the XPD patterns of B1s and N1s with the atomic structure of h-BN in Figure 3d thus proves that the transferred layer consists of large-area single orientation h-BN. The monolayer h-BN is consistent with Raman measurements, $i.e.$, the characteristic Raman peak at 1368 cm^{-1} with a full width at half maximum (FWHM) of 20 cm^{-1} (Figure S6).[23]

In order to demonstrate the protection functionality of the transferred h-BN, we developed a simple 'litmus' test that uses the oxidation of germanium in air as an indicator. Germanium is known to oxidize at temperatures above 370°C in air,[26] where it changes color from grey to light blue. In Figure 4 the color-change of a piece of Ge(111) wafer is shown during annealing from room temperature up to 610°C. We track 3 different 2×2 mm^2 regions, which are (i) pristine Ge, (ii) covered with PMMA and (iii) with PMMA/TOA/h-BN exfoliate that is folded to a double layer. The single fold minimizes the coincidence of defects in the single layer and thus enhance

the quality of protection.

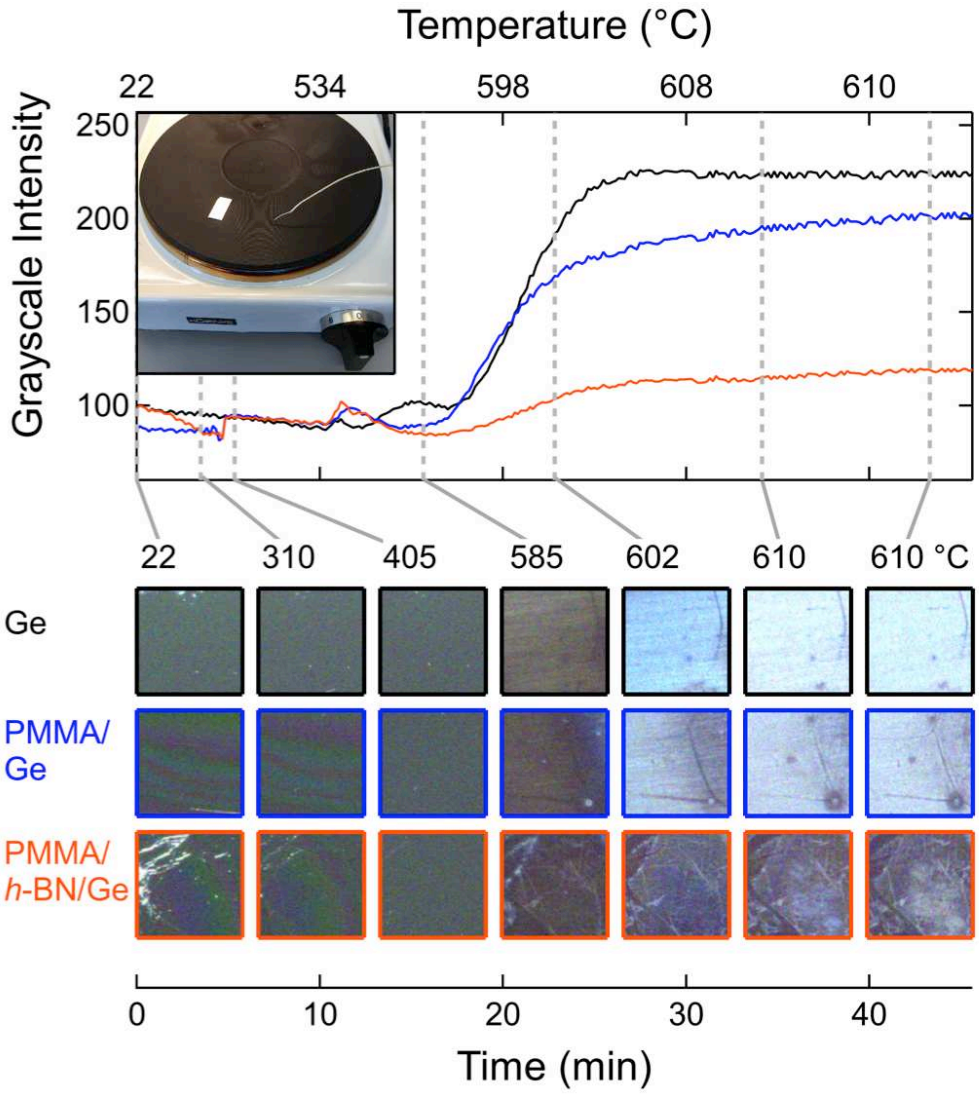

Figure 4: **Large-scale high temperature protection of Ge against oxidation by transferred h-BN.** The inset shows the heating plate with a piece of Ge wafer on top. PMMA and transferred PMMA/h-BN are placed on a Ge(111) surface. Top panel: Grayscale intensities of the camera images of Ge (black), PMMA/Ge (blue) and PMMA/h-BN/Ge (red) as a function of sample temperature and annealing time. The process involves three stages: (1) PMMA desorption at 300$\sim$350°C. (2) At $\sim$405°C, the three samples show the same color. (3) At 585°C, bare Ge and PMMA/Ge (after PMMA removal) start oxidizing and the colors of the surfaces turn bright blue (Ge bulk oxide formation), while PMMA/h-BN/Ge stays dark even after 10 min at 610°C. Bottom frame panel: Surface color changes of the three regions (7 frames each) vs. time and for temperatures from room temperature up to 610°C. All squares represent 2×2 mm^2. The color codes of the frame-boarders are the same as the traces in the top panel.

After sublimation of the PMMA at about 350°C the color is the same for all 3 spots. Upon further temperature increases, the optically visible oxidation process begins. However, the rates of color change are significantly different for the 3 regions, where it becomes clear that the h-BN covered spot resists oxidation up to 610°C. It is also observed that the PMMA-covered Ge area keeps the memory of having been covered, even though PMMA is no longer optically visible between 350 and 500°C. This test reflects the superior sealing behavior of atomically thin h-BN in extreme environments. Such membranes $e.g.$ allow the design of packing electronic components with tightest space constraints and best thermal energy dissipation properties. Furthermore, the Ge protection test signifies a viable low-cost tool for the characterization of the quality of macroscopic BN exfoliates. In particular, we point out that the test reveals sample inhomogeneities, therefore minimizing the need for analysis with expensive surface science methods. As such, it appears to be a useful benchmark method for optimization and comparison of material production and transfer processes.

Finally, we demonstrate the application of freestanding h-BN and v-BN exfoliates in membrane applications. State of the art TEM and scanning TEM (STEM) are known for their capability to measure h-BN and graphene with atomic resolution.[27] The h-BN layers are suspended over TEM grids (Cu quantifoil and SiN_x membranes) with diameters of the holes from 1.0 μm down to self-made 50 nm. Figure 5 shows spherical aberration-corrected TEM and STEM images, acquired at room temperature and with electron energies of 80 keV, which is between the boron and the nitrogen knock-on threshold in monolayer h-BN.[28,29] Figure 5a depicts a TEM grid with 1 μm holes covered by a single layer h-BN (dark-field TEM). The further zoom-in TEM image in Figure 5b shows freestanding monolayer h-BN with remaining PMMA/TOA traces. Atomically clean single layer h-BN patches can easily be found (Figure 5c). Figures 5D-5F demonstrate the application of single layer v-BN with 2 nm voids as conducting membranes in a potassium chloride (KCl) solution. Such membranes are potential candidates for blue energy harvesting like osmotic power generation as recently demonstrated for MoS_2 membranes[5] or may be used for ion separation.[30]

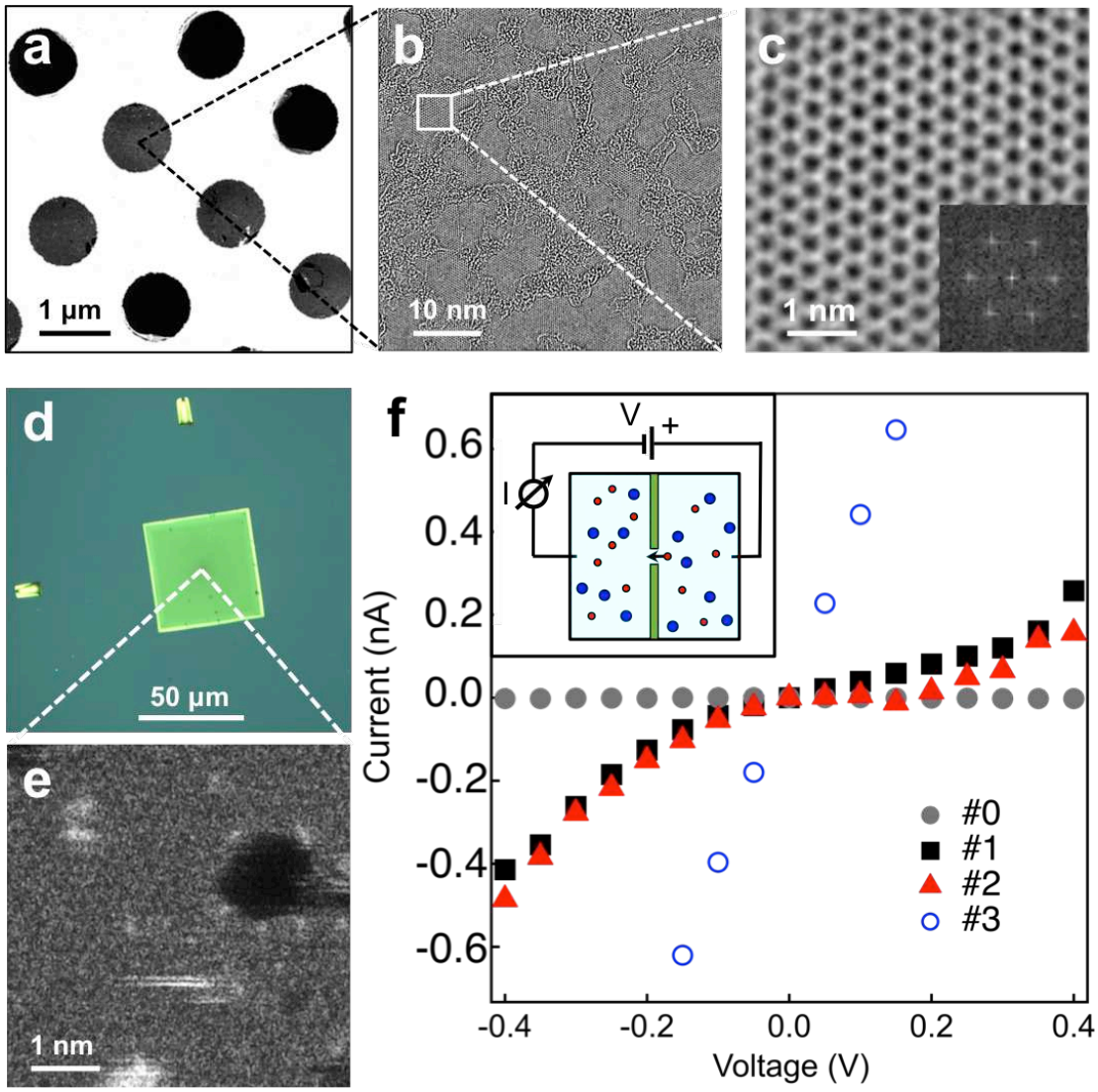

Figure 5: **Freestanding h-BN membranes.** (a) Dark-field TEM image of a large-area h-BN membrane suspended over a Cu quantifoil TEM grid. (b) Zoom-in TEM image displays freestanding single layer h-BN, with some transfer-related residues. (c) Further zoom-in high resolution (HR)TEM image: Single-crystalline BN honeycomb lattice with atomic resolution. Inset: Fast Fourier transform (FFT) of (c), confirming the crystalline structure with hexagonal symmetry. (d) Optical microscopy image of a h-BN membrane with 2 nm voids on a 20 nm SiN_x membrane with 50 nm hole in the middle. (e) HR-STEM image of a h-BN membrane with a 2 nm void. (f) Current vs. voltage characteristic of 4 different v-BN membrane samples in 10 mM KCl solutions at pH 8. The inset shows the sketch of the setup. All TEM and STEM images are taken at 80 keV electron energy and at room temperature.

In our ion conductivity setup,[31] a circular 50 nm hole in 20 nm thick SiN membrane is covered with v-BN membrane (Figure 5d). In Figure 5e a 5×5 nm^2 STEM image with one void is shown.

Measurements of current vs. voltage I-V characteristics demonstrate that ion conductivity across such voidal membranes can be measured. In Figure 5f conductivities of 0.01 M KCl, pH=8 at room temperature are displayed for four different v-BN membranes. Below cell voltages of $\pm$200 mV, conductivities of (-1$\pm$3) $\times$ 10^{-3}, 0.48$\pm$0.07, 0.36$\pm$0.18 and 4.24$\pm$0.07 nS are obtained (for details see part 7 in SI).[32–34] From the conductance of the KCl solution and the void dimensions, we estimate the number of voids or ion channels to be 0, 2, 1 and 16 for the four membrane I-V curves shown in Figure 5f. The hole quantities are in the same order of magnitude as expected from the nominal v-BN void density before transfer of 2.3×10^{-3}nm^{-2}, or 3 to 6 voids on a membrane with diameter of 50 nm. Given the uncertainties in relating the measured conductance to the void density we consider the conductivities of membrane samples ($^{\#}1$ and $^{\#}2$ in Figure 5f) to be close to the expectation. At variance to solid state electrolyte boron nitride membrane applications[35] we also find ion tight membranes ($^{\#}0$). $^{\#}3$ with 4 nS conductivity likely corresponds to a broken membrane.

Conclusions

A method for transfer of centimeter-sized single-orientation h-BN with or without surface modifications (nanovoids) from single-crystalline Rh(111) thin films is presented. The process involves two steps, a TOA^+ treatment of the h-BN surface, followed by hydrogen driven delamination. Advantages of this non-destructive isolation of CVD-grown h-BN include: (1) Scalability; (2) Substrate recycling; (3) Sustaining functionalizations that rely on the metal substrate like the "can-opener" effect may be performed. In order to confirm the application potential of these 2D layers we demonstrate their thermal oxidation protection capability in air and the use as mono-atomic membranes with and without ion channels in aqueous solutions.

Methods

Instrumentation for sample fabrication

The CVD growth of h-BN was performed in an UHV system with a base pressure of 1×10^{-10} mbar. For the high temperature CVD fabrication of the h-BN nanomesh we employed a standard procedure on 150 nm single-crystalline Rh(111)/YSZ/Si films at 4-inch wafer scale.[11,12] For the 2 nm void-generation we used a Specs IQP 10/35 Penning-type ion source run at lowest acceleration potential. The intergrated sputter charge density was 250 nC/cm^2.

Two-step TOA$^+$-assisted electrochemical process

The first step involves a three-electrode electrochemical setup. It consists of a h-BN/Rh sample as working electrode, a Pt wire as counter electrode and an Ag-wire as reference electrode in Ar degassed 0.1 M TOABr/acetonitrile. The reference potential vs. Ag-wire was kept at -1.9 V for 10 minutes, followed by a potential of -0.2 V vs. Ag-wire for 20 seconds. Subsequently, the sample was rinsed with acetonitrile and spin-coated with 4 wt.% PMMA (495 K). The second step involves the PMMA/TOA/h-BN/Rh sample as working electrode and a graphite rod as counter electrode in 1.0 M KCl solution. A negative voltage between -3 V and -6 V was applied to the sample while it was gradually immersed into the solution. H_2 bubbles form at the h-BN/Rh interface and delaminate the h-BN/TOA/PMMA film from the substrate. The delaminated h-BN/TOA/PMMA film was then rinsed in ultra-pure water (Milli-Q Advantage A10) and transferred on a clean 80 nm SiO_2/Si substrate. In the next step, the PMMA was removed via a sequence of acetone/ethanol baths at 370 K and gradual anneal in air up to 600 K for 3 hours. Two types of TEM grids were used: (1) Cu quantifoil with empty hole size of 1000 nm and interval distance of holes of 800 nm (Figure 5a) and (2) SiN_x with a thickness of 20 nm and a single hole with 50 nm in diameter in the middle (Figure 5d). The TEM grids were coated with 25 nm Pt prior to the transferred layer deposition. The Pt acts as a catalyst that reduces the PMMA disintegration temperature and improves the PMMA removal-efficiency.[36] After transfer, the PMMA/TOA/h-BN/grids were

slowly heated up in air to 600 K for 5 hours to remove PMMA/TOA. The Rh(111) film substrate was then put back to the UHV system and heated up to 800 K before XPS and low-energy electron diffraction (LEED) measurements.

Sample characterizations

All sample characterizations were carried out at room temperature.

The scanning tunneling microscopy (STM) measurements were accomplished with an Omicron variable temperature STM (VT-STM) with electrochemically etched tungsten tips. All STM images were taken in constant-current mode.

Optical images were acquired using a Leica DMV2500 stereomicroscope with a maximum magnification of 2500×. Sequential frame acquisition was performed using procedures written with the Leica Self-Development Kit package, and the frames were subsequently stitched using the Fiji image-processing package.

XPS, x-ray photoelectron diffraction (XPD) and LEED measurements were carried out on a user-modified Vacuum Generators ESCALAB 220[37] with a Mg Kα lab source at an energy of $\hbar\omega = 1253.6$ eV. X-ray photo-emission electron microscopy (X-PEEM) images were recorded at the boron K-edge at the Surface/Interface: Microscopy (SIM) beamline of the SLS.

Raman measurements were performed with a Thermo Scientific DXR^{TM} 2 Raman Microscope equipped with CCR1000 Linkam at 455 nm excitation wavelength. Scanning electron microscopy (SEM) in Figure S2 were measured using a Zeiss Supra 50 VP field-emission SEM equipped with secondary, back-scattered electron and EDX detectors at energies between 2 $\sim$ 2.5 keV.

TEM and STEM images were measured on an aberration-corrected (with double Cs corrector) FEI Titan Themis TEM (60-300) operated at an 80 kV acceleration voltage. For HRTEM imaging, a spherical aberration (Cs) of about -20 μm was applied, combined with a monochromate incident illumination to reduce the effects of chromatic aberration, for an optical setup capable of 1 Å resolution or better. Images are shown with focus adjusted to give a white atom contrast[38] which, when imaging clean uncontaminated monolayer, allows the phase contrast HRTEM image to be directly

interpreted as atomic positions. (S)TEM image Processing: Raw TEM images were filtered by using a bandpass filter between 1 and 100 pixels. These filtered images were then blurred out using a Gaussian blur function with a diameter of 1.2 pixels to enhance visual inspections.

Nanofluidic transport experiments were performed using the setup described previously.[31] After mounting in the chamber, chips were wetted with H_2O:ethanol (1:1) solution for 30 minutes. Nanofluidic measurements were performed by taking the current-voltage response (IV characteristics) of the nanovoid in salt solutions of potassium chloride (KCl, Sigma Aldrich) using an Axopatch 200B patch-clamp amplifier (Molecular Devices, Inc. Sunnyvale, CA) with voltage range from -1.0 to 1.0 V.

Associated Content

Supporting Information

The following Supporting Information is available free of charge on the ACS Publications website.

Transfer methods comparison, re-usability of substrates, characterization details, ion conductivity model and supporting data (PDF).

Author Information

Corresponding Author

*E-mail: huanyao.cun@epfl.ch

ORCID

Huanyao Cun: 0000-0002-5225-9861

Thomas Greber: 0000-0002-5234-1937

Notes

The authors declare no competing financial interest.

Acknowledgements

Financial support by the Swiss National Science Foundation, by the EC under the Graphene Flagship (contract no. CNECT-ICT-604391) is gratefully acknowledged. We gratefully thank Prof. Dr. Wlodek Strupinski and Dr. Aleksandra Krajewska from the Institute of Electronic Materials Technology in Warsaw for introducing the electrochemical graphene transfer from Cu foil. We thank Dr. Qasim Imtiaz, Manouchehr Nadjafi and Dr. Miroslav Haluska from ETH Zürich for introducing the Raman instruments. Part of this work was performed at the Surface/Interface:Microscopy (SIM) beam line of the Swiss Light Source, Paul Scherrer Institut (PSI), Villigen, Switzerland. We thank Marianna Lorenzo and Dr. Jean-Nicholas Longchamp for Pt coating and fruitful discussions, Anja Weber (PSI) for providing the SiO_2/Si substrates, and the Centre Interdisciplinaire de Microscopie Electronique (CIME) at the EPFL Lausanne and the Center for Microscopy and Image Analysis of the University of Zurich (Dr. Andres Käch) for access to electron microscopes.

Supporting Information

Table of Contents

1. Transfer of h-BN flakes with "bubbling-only" method

Four different characterization methods are applied for the same transferred BN flakes on 80 nm SiO_2 with "bubbling-only, no TOA-assist" approach by SEM, X-PEEM, optical microscopy (OM) and sample averaging XPS, as shown in Figure S1. The BN flakes marked with blue and red circles are the same in all images recorded in 3 different microscopes.

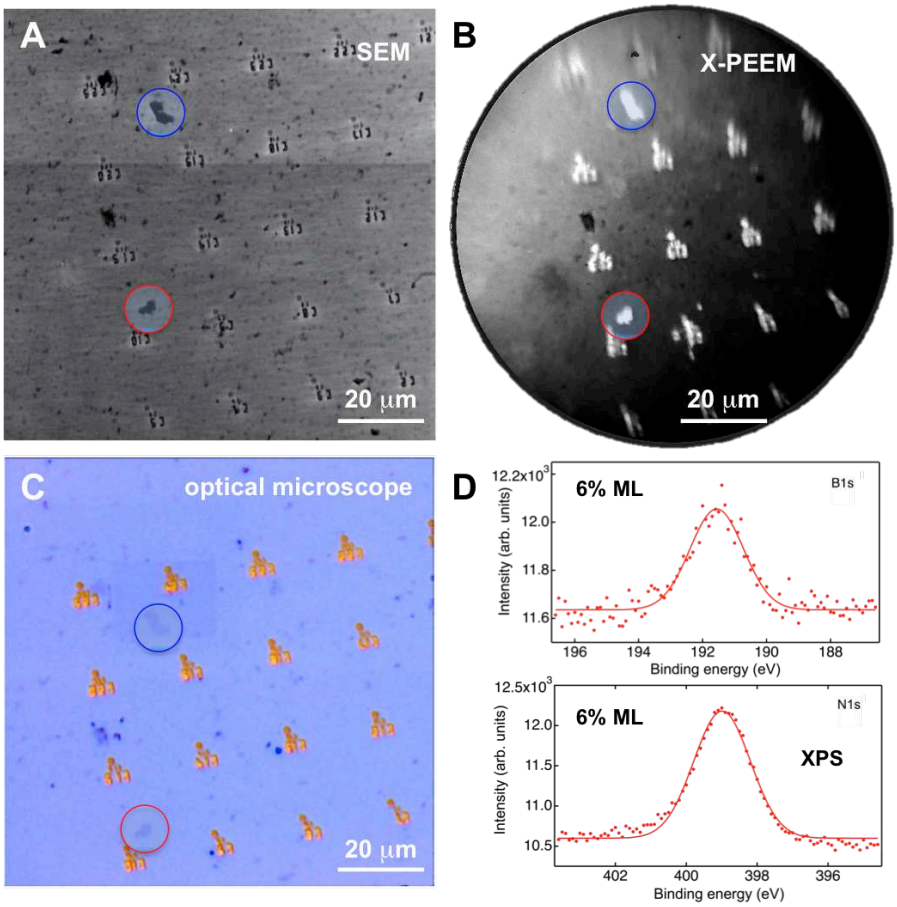

Figure 6: **Characterization of micrometer-sized h-BN flakes on 80 nm SiO_2 exfoliated from h-BN/Rh(111) without TOA^+-treatment.** The circles with the same colors (blue or red) in (A), (B) and (C) indicate the same individual flakes, as identified by gold markers on the SiO_2 substrate. (A) SEM. (B) X-PEEM image recorded at the boron K-edge (data taken at the SIM beamline of the Swiss Light Source). (C) Optical microscopy. (D) XPS B1s and N1s peaks of the same transferred BN sample on SiO_2.

2. Regrowth of h-BN on recycled Rh(111)

Rh(111) substrates after h-BN transfer were characterized by LEED (Figure S2B), XPS (Figure S2D and S2E) and atomic force microscopy (AFM) (Figure S2F). After h-BN delamination, the Rh(111) film was transferred back to UHV for characterization and a new preparation of h-BN monolayer by high-temperature CVD with borazine $(HBNH)_3$ as precursor.[12,13] The quality of second growth h-BN is as good as the preceding preparation as can be judged from LEED (Figure S2A and S2C) and XPS (Figure S2D and S2E).

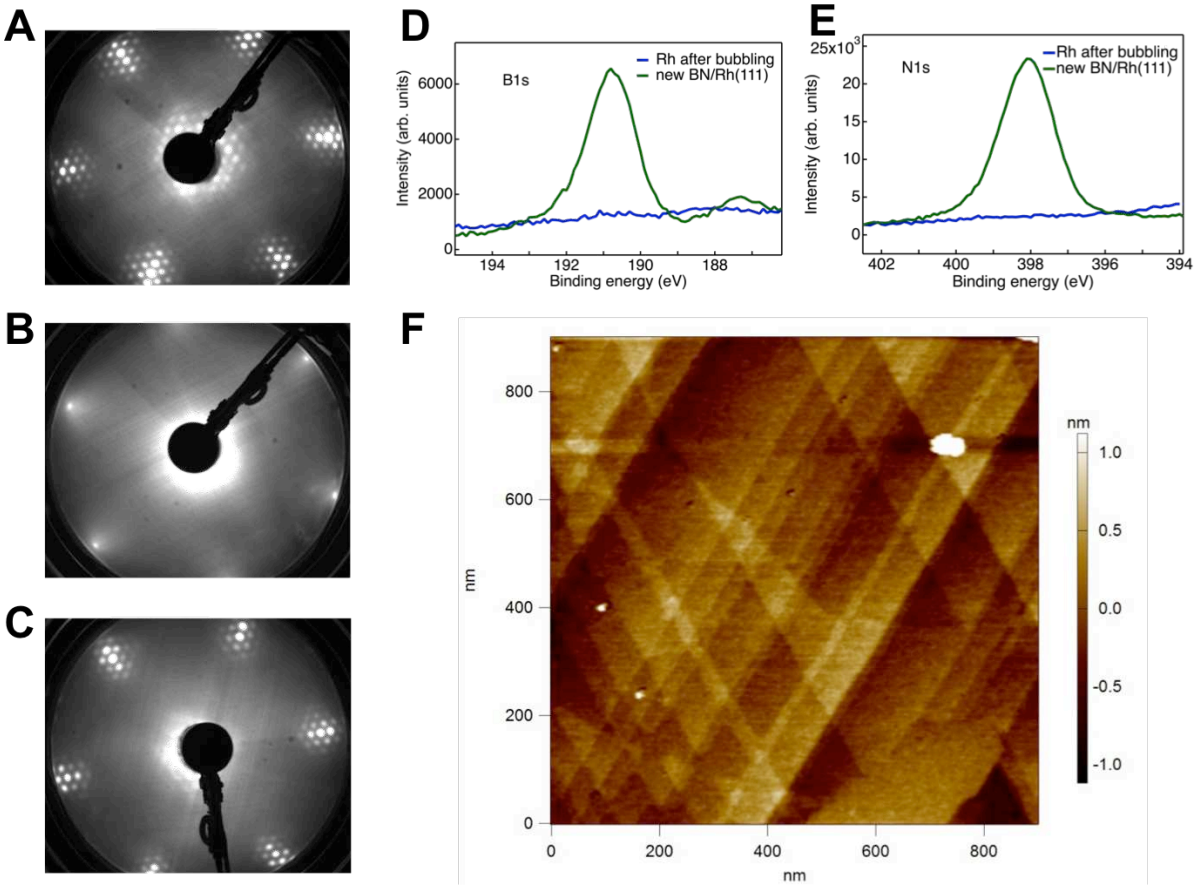

Figure 7: **Regrowth of h-BN nanomesh on used Rh(111) substrates.** (A-C) LEED patterns. (A) Pristine h-BN with the 13×13 BN on 12×12 Rh superstructure spots. (B) Rh(111) substrate after "bubbling" transfer. (C) Second growth of h-BN/Rh(111). XPS B1s (D) and N1s (E) peaks on the Rh film after transfer (blue) and regrown h-BN/Rh (green). (F) 900×900 nm^2 AFM image at room temperature shows the clean surface of a Rh(111) substrate after the h-BN transfer.

3. Survey spectra of h-BN monolayer before and after transfer

The XPS survey spectra of h-BN monolayer in Figure 3 of the main text were measured before (h-BN/Rh(111)) and after (h-BN/SiO_2) the transfer, as displayed in Figure S3.

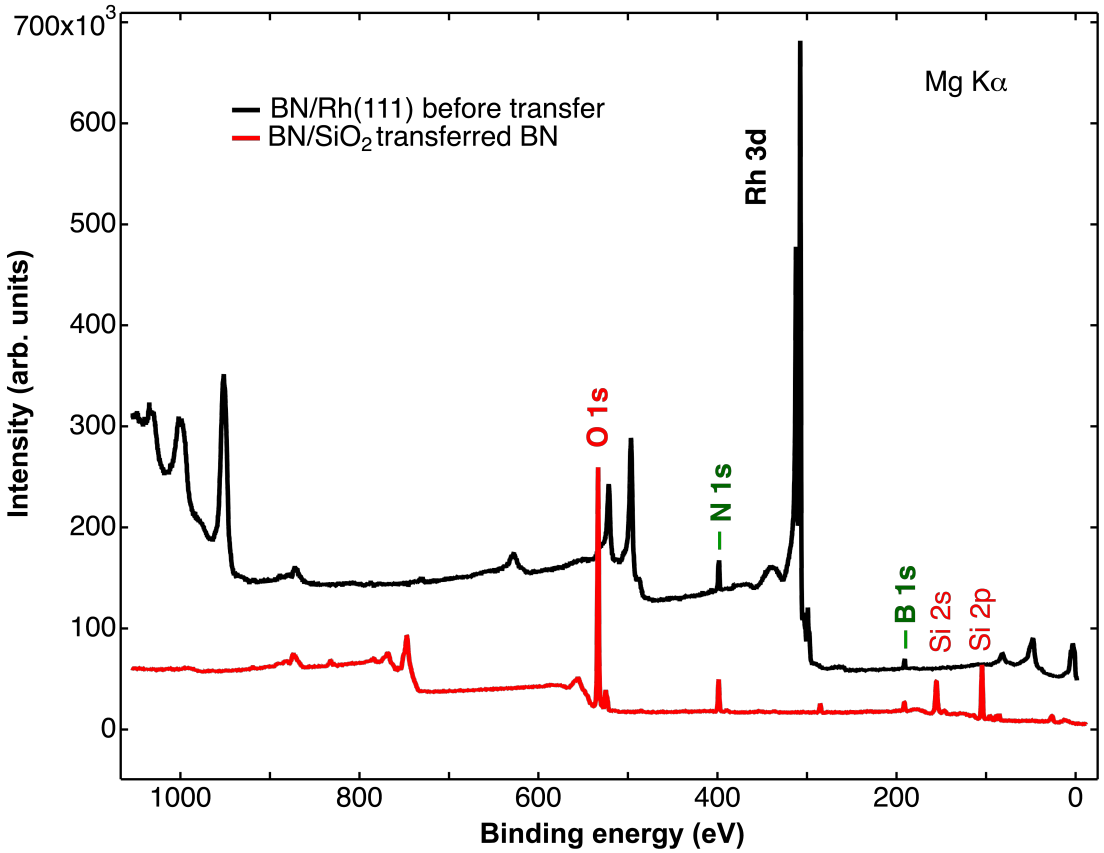

Figure 8: **Survey spectra of h-BN monolayer before and after transfer.** Mg Kα XPS ($\hbar\omega = 1253.6$ eV) survey spectra with the same source and analyzer settings show the difference between before (black, h-BN/Rh(111)) and after (red, h-BN/SiO_2) membrane transfer. The transfer rate is above 95%, which is confirmed by the B1s and N1s peaks of h-BN/SiO_2 after transfer.

4. Determination of the transfer rate of h-BN monolayer

In order to determine the transfer rate of h-BN, three sets of XPS (MgKα, $\hbar\omega = 1253.6$ eV) measurements are carried out for pristine h-BN/Rh(111), transferred h-BN/SiO_2, and used Rh(111) substrates after h-BN delamination, respectively. The three samples are typically annealed to 950

K (for h-BN/Rh(111) and used Rh(111) substrates) and 650 K for transferred h-BN/SiO_2. The B1s and N1s peaks of these three samples (derived from the same h-BN/Rh preparation) are integrated individually (I_{tot}, I_{tra} and I_{rem}). The peaks are measured with the same pass energy, sweep numbers and scan time. The peak integrals of the core levels of B1s (I_{totB}) and N1s (I_{totN}) are 100% for a pristine h-BN monolayer. The B1s and N1s peak intensity ratios of transferred h-BN/SiO_2 (I_{traB} and I_{traN}) and pristine h-BN/Rh(111) are defined as the transfer rate σ_{tra}:

$$\sigma_{tra} = \frac{I_{traB(N)}}{I_{totB(N)}}$$

The remaining BN ratio (σ_{rem}) on the bubbled Rh(111) is defined as:

$$\sigma_{rem} = \frac{I_{remB(N)}}{I_{totB(N)}}$$

Therefore the lost BN ratio can be calculated as:

$$\sigma_{los} = 1 - \sigma_{tra} - \sigma_{rem}$$

Thus the removed BN ratio σ_{remove} = σ_{tra} + σ_{los}. Without loss, the transferred BN ratio σ_{tra} is the same as the removed BN ratio σ_{remove}. The correlation between transferred BN vs. removed BN based on 57 experiments is displayed in Figure S4. The light blue data points correspond to transfers without TOA^+-treatment, while dark blue and red colors are the experiments with TOA^+-treatment. Clearly, the electrochemical "bubbling" method without TOA^+-assist does not lead to complete h-BN monolayer transfer. The upper-right corner with σ_{tra}/σ_{remove} = 1:1 is the ultimate goal for the transfer.

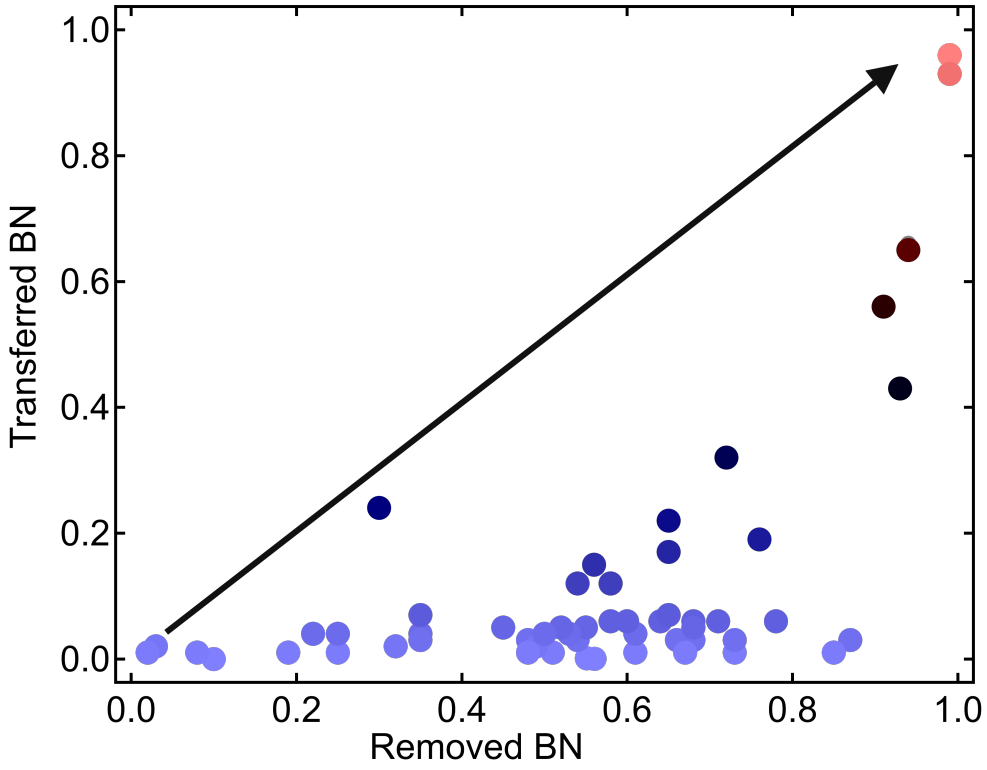

Figure 9: **Transfer rates vs. remove rates for different h-BN transfer samples.** The Y axis represents the transferred BN and X axis stands for the removed BN. The light blue color represents the transfers without TOA^+-assisted "bubbling", while transfer rates above 60% have only been obtained by TOA^+-assisted transfer. The black arrow indicates the maximum transfer at a given removal and the arrowhead points to the goal of "complete transfer".

5. Optical microscopy of continuous h-BN monolayer with TOA^+-assisted process

The continuous h-BN monolayers transferred on 80 nm SiO_2 can be observed with optical microscopy at room temperature after removal of PMMA, as shown in Figure S5. The size of transferred BN monolayer is 9.5×9.5 mm^2.

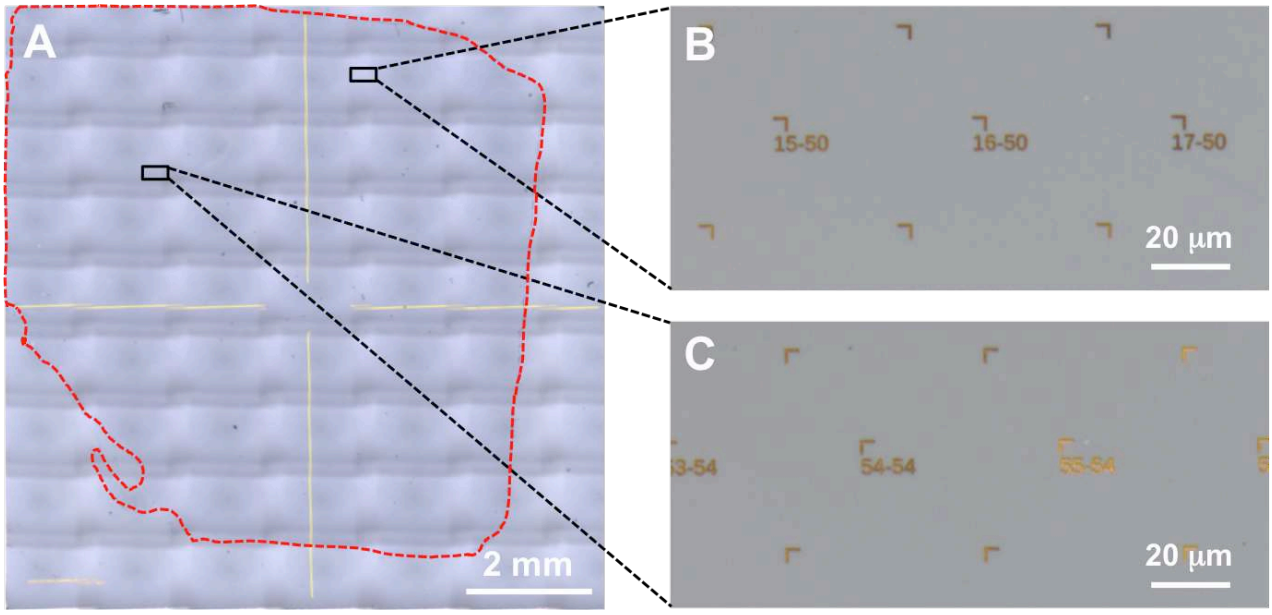

Figure 10: **Optical microscopy images of transferred h-BN/SiO_2/Si.** (A) Optical microscopy overview image shows the entire transferred continuous h-BN monolayer with centimeter-size. The image was obtained by stitching multiple optical images with 150× magnification. The slightly darker region is the h-BN-covered area, which is marked with dashed red lines to guide the eyes (square shape with a cut-edge at left-bottom). (B) and (C) are two zoom-in images with 2000× magnification. The gold markers on SiO_2 are used for localizing specific spots on the surface in different instruments.

6. Raman spectrum

Raman spectra were measured with beam wavelengths of 455 nm. The fingerprint peak of h-BN at 1368 cm^{-1} is clearly identified[23] with an average full width at half maximum (FWHM) of 20 cm^{-1}.

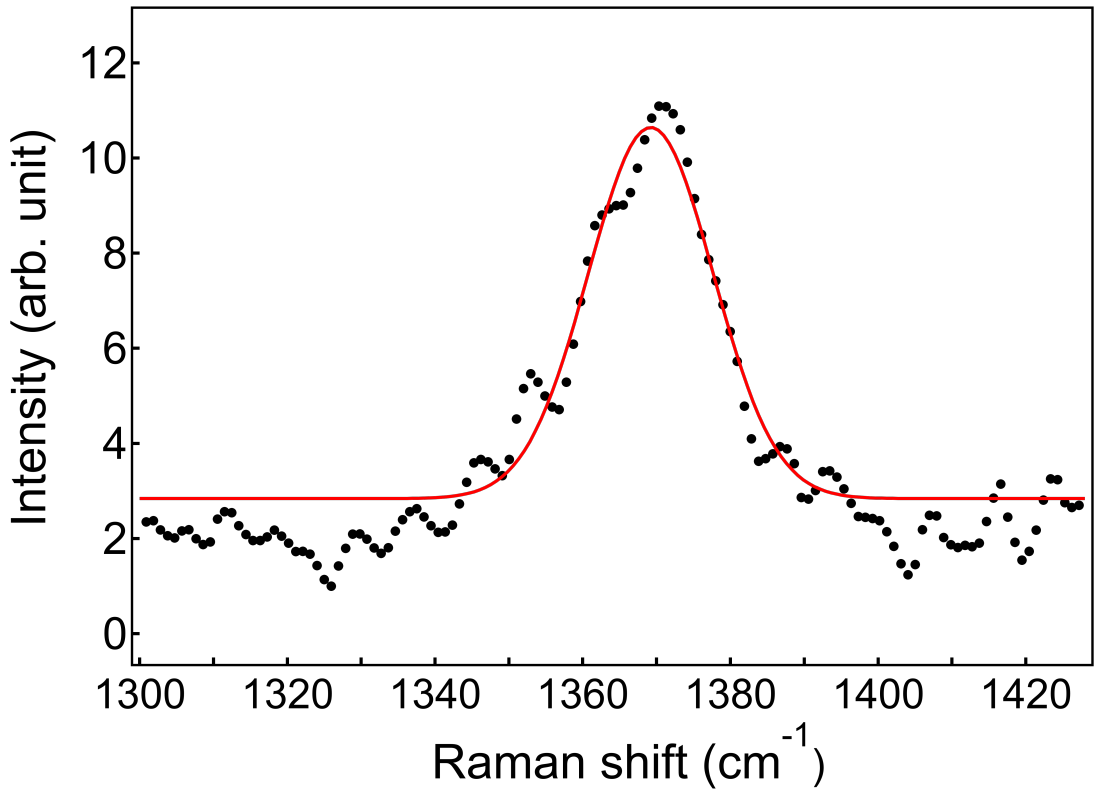

Figure 11: **Representative Raman spectrum of transferred h-BN/SiO$_2$/Si sample.** The Raman spectrum of h-BN/SiO$_2$/Si sample with transfer rate of 95 % shows the fingerprint peak of h-BN monolayer at 1368 cm^{-1} at wavelength of 455 nm. The red curves represent the Gaussian fits.

7. Ion conductivity model

The void density of voidal boron nitride (v-BN) membranes used in the ion conductivity experiments may be estimated from theoretical considerations. According to the model first proposed by Hall[32] and later adopted by Kowalcyzk et al.[33] and Lee et al.,[34] the conductivity of an ion channel is given by

$$G = \sigma \left(\frac{4L}{\pi D^2} \frac{1}{1 + \frac{4l_{Du}}{D}} + \frac{1}{D} \right)^{-1} \tag{1}$$

where σ is the bulk conductivity of the electrolyte, l_{Du} is the Debye length, L is the nominal membrane thickness and D the diameter of an ion channel. The first term in equation (1) is the

transfer conductance, and the second term is the access conductivity G_A. For the given nonporous in a KCl electrolyte with σ= 0.15 S/m that has a Debye length l_{Du} of 3 nm, a nominal membrane thickness L of 1.4 nm and a nanopore diameter D of 2 nm, we get a conductivity of 0.27 nS per nanopore. Thus we estimate the "effective" number of voids to be 0, 1.8, 1.3 and 15.9 for the shown 4 membranes in Figure 5F. In comparison, from the nominal void density in the applied v-BN of 2.3×10^{-3}nm^{-2}, an average void number of 4.5 per membrane is expected.

References

1. Geim, A. K.; Grigorieva, I. V. Van der Waals heterostructures. *Nature* **2013**, *499*, 419–425.

2. Mak, K. F.; Lee, C.; Hone, J.; Shan, J.; Heinz, T. F. Atomically thin $\mathrm{MoS_2}$: A new direct-gap semiconductor. *Phys. Rev. Lett.* **2010**, *105*, 136805.

3. Siria, A.; Poncharal, P.; Biance, A.; Fulcrand, R.; Blase, X.; Purcell, S. T.; Bocquet, L. Giant osmotic energy conversion measured in a single transmembrane boron nitride nanotube. *Nature* **2013**, *494*, 455–458.

4. Mertens, S.; Hemmi, A.; Muff, S.; Gröning, O.; Feyter, S. D.; Osterwalder, J.; Greber, T. Switching stiction and adhesion of a liquid on a solid. *Nature* **2016**, *534*, 676–679.

5. Feng, J.; Graf, M.; Liu, K.; Ovchinnikov, D.; Dumcenco, D.; Heiranian, M.; Nandigana, V.; Aluru, N. R.; Kis, A.; Radenovic, A. Single-layer MoS_2 nanopores as nanopower generators. *Nature* **2016**, *536*, 197–200.

6. Dean, C. R.; Young, A. F.; Meric, I.; Lee, C.; Wang, L.; Sorgenfrei, S.; Watanabe, K.; Taniguchi, T.; Kim, P.; Shepard, K. L. *et al.* Boron nitride substrates for high-quality graphene electronics. *Nat. Nanotechnol.* **2010**, *5*, 722–726.

7. Gao, Y.; Ren, W.; Ma, T.; Liu, Z.; Zhang, Y.; Liu, W.; Ma, L.; Ma, X.; Cheng, H.-M. Repeated and controlled growth of monolayer, bilayer and few-Layer hexagonal boron nitride on Pt foils. *ACS Nano* **2013**, *7*, 5199–5206.

8. Jang, A.-R.; Hong, S.; Hyun, C.; Yoon, S. I.; Kim, G.; Jeong, H. Y.; Shin, T. J.; Park, S. O.; Wong, K.; Kwak, S. K. *et al.* Wafer-scale and wrinkle-free epitaxial growth of single-orientated multilayer hexagonal boron nitride on sapphire. *Nano Lett.* **2016**, *16*, 3360–3366.

9. Oh, H.; Jo, J.; Tchoe, Y.; Yoon, H.; Lee, H. H.; Kim, S.-S.; Kim, M.; Sohn, B.-H.; Yi, G.-C. Centimeter-sized epitaxial h-BN films. *NPG Asia Mater.* **2016**, *8*, e330.

10. Gsell, S.; Fischer, M.; Schreck, M.; Stritzker, B. Epitaxial films of metals from the platinum group (Ir, Rh, Pt and Ru) on YSZ-buffered Si(111). *J. Cryst. Growth* **2009**, *331*, 3731–3736.

11. Hemmi, A.; Bernard, C.; Cun, H. Y.; Roth, S.; Klöckner, M.; Kälin, T.; Weinl, M.; Gsell, S.; Schreck, M.; Osterwalder, J. *et al.* High quality single atomic layer deposition of hexagonal boron nitride on single crystalline Rh(111) four-inch wafers. *Rev. Sci. Instrum.* **2014**, *85*, 035101.

12. Corso, M.; Auwärter, W.; Muntwiler, M.; Tamai, A.; Greber, T.; Osterwalder, J. Boron nitride nanomesh. *Science* **2004**, *303*, 217–220.

13. Berner, S.; Corso, M.; Widmer, R.; Groening, O.; Laskowski, R.; Blaha, P.; Schwarz, K.; Goriachko, A.; Over, H.; Gsell, S. *et al.* Boron nitride nanomesh: Functionality from a corrugated monolayer. *Angew. Chem. Int. Ed.* **2007**, *46*, 5115–5119.

14. Díaz, J. G.; Ding, Y.; Koitz, R.; Seitsonen, A. P.; Iannuzzi, M.; Hutter, J. Hexagonal boron nitride on transition metal surfaces. *Theor. Chem. Acc.* **2013**, *132*, 1350–1366.

15. Widmer, R.; Berner, S.; Gröning, O.; Brugger, T.; Osterwalder, J.; Greber, T. Electrolytic in situ STM investigation of h-BN-Nanomesh. *Electrochem. Commun.* **2007**, *9*, 2484–2488.

16. Brugger, T.; Ma, H.; Iannuzzi, M.; Berner, S.; Winkler, A.; Hutter, J.; Osterwalder, J.; Greber, T. Nanotexture switching of single-layer hexagonal boron nitride on rhodium by intercalation of hydrogen atoms. *Angew. Chem. Int. Ed.* **2010**, *49*, 6120–6124.

17. Cun, H. Y.; Iannuzzi, M.; Hemmi, A.; Roth, S.; Osterwalder, J.; Greber, T. Immobilizing individual atoms beneath a corrugated single layer of boron nitride. *Nano Lett.* **2013**, *13*, 2098–2103.

18. Cun, H. Y.; Iannuzzi, M.; Hemmi, A.; Osterwalder, J.; Greber, T. Two-Nanometer voids in single-layer hexagonal boron nitride: Formation via the ”can-opener” effect and annihilation by self-healing. *ACS Nano* **2014**, *8*, 7423–7431.

19. Cun, H. Y.; Iannuzzi, M.; Hemmi, A.; Osterwalder, J.; Greber, T. Implantation length and thermal stability of interstitial Ar stoms in boron nitride nanotents. *ACS Nano* **2014**, *8*, 1014–1021.

20. Koefoed, L.; Kongsfelt, M.; Ulstrup, S.; Čabo, A. G.; Cassidy, A.; Whelan, P. R.; Bianchi, M.; Dendzik, M.; Pizzocchero, F.; Jørgensen, B. *et al.* Facile electrochemical transfer of large-area single crystal epitaxial graphene from Ir(111). *J. Phys. D: Appl. Phys.* **2015**, *48*, 115306.

21. Wang, Y.; Zheng, Y.; Xu, X.; Dubuisson, E.; Bao, Q.; Lu, J.; Loh, K. P. Electrochemical delamination of CVD-Grown graphene film: Toward the recyclable use of copper catalyst. *ACS Nano* **2011**, *5*, 9927–9933.

22. Ciuk, T.; Pasternak, I.; Krajewska, A.; Sobieski, J.; Caban, P.; Szmidt, J.; Strupinski, W. Properties of chemical vapor deposition graphene transferred by high-speed electrochemical delamination. *J. Phys. Chem. C* **2013**, *117*, 20833–20837.

23. Gorbachev, R. V.; Riaz, I.; Nair, R. R.; Jalil, R.; Britnell, L.; Belle, B. D.; Hill, E. W.; Novoselov, K. S.; Watanabe, K.; Taniguchi, T. *et al.* Hunting for monolayer boron nitride: Optical and Raman signatures. *Small* **2011**, *4*, 465–468.

24. Auwärter, W.; Kreutz, T.; Greber, T.; Osterwalder, J. XPD and STM investigation of hexagonal boron nitride on Ni(111). *Surf. Sci.* **1999**, *429*, 229–236.

25. Roth, S.; Greber, T.; Osterwalder, J. Some Like It Flat: Decoupled h-BN Monolayer Substrates for Aligned Graphene Growth. *ACS Nano* **2016**, *10*, 11187–11195.

26. Sahari, S. K.; Ohta, A.; Matsui, M.; Mishima1, K.; Murakami, H.; Higashi, S.; Miyazaki, S. Kinetics of thermally oxidation of Ge(100) surface. *J. Phys.: Confer. Seri.* **2013**, *417*, 012014.

27. Krivanek, O. L.; Chisholm, M. F.; Nicolosi, V.; Pennycook, T. J.; Corbin, G. J.; Dellby, N.; Murfitt, M. F.; Own, C. S.; Szilagyi, Z. S.; Oxley, M. P. *et al.* Atom-by-atom structural and chemical analysis by annular dark-field electron microscopy. *Nature* **2010**, *464*, 571–574.

28. Meyer, J. C.; Chuvilin, A.; Algara-Siller, G.; Biskupek, J.; Kaiser, U. Selective sputtering and atomic resolution imaging of atomically thin boron nitride membranes. *Nano Lett.* **2009**, *9*, 2683–2689.

29. Kotakoski, J.; Jin, C. H.; Lehtinen, O.; Suenaga, K.; Krasheninnikov, A. V. Electron knock-on damage in hexagonal boron nitride monolayers. *Phys. Rev. B* **2010**, *82*, 113404.

30. O'Hern, S. C.; Boutilier, M. S. H.; Idrobo, J.-C.; Song, Y.; Kong, J.; Laoui, T.; Atieh, M.; Karnik, R. Selective ionic transport through tunable subnanometer pores in single-layer graphene membranes. *Nano Lett.* **2014**, *14*, 1234–1241.

31. Liu, K.; Feng, J.; Kis, A.; Radenovic, A. Atomically thin molybdenum disulfide nanopores with high sensitivity for DNA translocation. *ACS Nano* **2014**, *8*, 2504–2511.

32. Hall, J. E. Access resistance of a small circular pore. *J. Gen. Physiol.* **1975**, *66*, 531–532.

33. Kowalczyk, S. W.; Grosberg, A. Y.; Rabin, Y.; Dekker, C. Modeling the conductance and DNA blockade of solid-state nanopores. *Nanotechnology* **2011**, *22*, 315101.

34. Lee, C.; Joly, L.; Siria, A.; Biance, A.-L.; Fulcrand, R.; Bocquet, L. Large apparent electric size of solid-state nanopores due to spatially extended surface conduction. *Nano Lett.* **2012**, *12*, 4034–4044.

35. Hu, S.; Lozada-Hidalgo, M.; Wang, F. C.; Mishchenko, A.; Schedin, F.; Nair, P. R.; Hill, E. W.; Boukhvalov, D. W.; Katsnelson, M. I.; Dryfe, R. A. W. *et al.* Proton transport through one-atom-thick crystals. *Nature* **2014**, *516*, 227–230.

36. Longchamp, J. N.; Escher, C.; Fink, H. W. Ultraclean freestanding graphene by platinum-metal catalysis. *J. Vac. Sci. Technol. B* **2013**, *31*, 020605.

37. Greber, T.; Raetzo, O.; Kreutz, T.; Schwaller, P.; Deichmann, W.; Wetli, E.; Osterwalder, J. A photoelectron spectrometer for k-space mapping above the Fermi level. *Rev. Sci. Instrum.* **1997**, *68*, 4549–4554.

38. Ryu, G. H.; Park, H. J.; Ryou, J.; Park, J.; Lee, J.; Kim, G.; Shin, H. S.; Bielawski, C. W.; Ruoff, R. S.; Hong, S. *et al.* Atomic-scale dynamics of triangular hole growth in monolayer hexagonal boron nitride under electron irradiation. *Nanoscale* **2015**, *7*, 10600–10605.

Graphical TOC Entry